symmetry

MDPI

Article

A Third Angular Momentum of Photons

Pathik Sahoo [1,2], Pushpendra Singh [1,2], Jhimli Manna [2], Ravindra P. Singh [3], Jonathan P. Hill [1], Tomonobu Nakayama [1], Subrata Ghosh [4,5] and Anirban Bandyopadhyay [1,2,*]

1 International Center for Materials Nanoarchitectronics (MANA), NIMS, 1-2-1 Sengen, Tsukuba 3050047, Ibaraki, Japan
2 Research Center for Advanced Measurement and Characterization (RCAMC), NIMS, 1-2-1 Sengen, Tsukuba 3050047, Ibaraki, Japan
3 Quantum Science & Technology Laboratory, Physical Research Laboratory, Navrangpura, Ahmedabad 380009, Gujarat, India
4 Chemical Science and Technology Division, CSIR-North East Institute of Science and Technology, NEIST, Jorhat 785006, Assam, India
5 Academy of Scientific and Innovative Research (AcSIR), Ghaziabad 201002, Uttar Pradesh, India
* Correspondence: anirban.bandyo@gmail.com

Abstract: Photons that acquire orbital angular momentum move in a helical path and are observed as a light ring. During helical motion, if a force is applied perpendicular to the direction of motion, an additional radial angular momentum is introduced, and alternate dark spots appear on the light ring. Here, a third, centrifugal angular momentum has been added by twisting the helical path further according to the three-step hierarchical assembly of helical organic nanowires. Attaining a third angular momentum is the theoretical limit for a photon. The additional angular momentum converts the dimensionless photon to a hollow spherical photon condensate with interactive dark regions. A stream of these photon condensates can interfere like a wave or disintegrate like matter, similar to the behavior of electrons.

Keywords: light–matter interaction; phase singularity; optical vortex; helical nanowire

Citation: Sahoo, P.; Singh, P.; Manna, J.; Singh, R.P.; Hill, J.P.; Nakayama, T.; Ghosh, S.; Bandyopadhyay, A. A Third Angular Momentum of Photons. *Symmetry* **2023**, *15*, 158. https://doi.org/10.3390/sym15010158

Academic Editor: Giovanni Angiulli

Received: 18 December 2022
Revised: 30 December 2022
Accepted: 3 January 2023
Published: 5 January 2023

Main Text

Vortices are ripples in the homogeneous distribution of fields. They diminish gradually after giving insights into 4D spacetime in astrophysics [1], form lattices in superconductors [2], operate algorithms using electromechanical nested rhythms [3], etc. All vortices dissipate and eventually disappear. Here, we have reshaped vortices of photons [4–10] into a 3D particle, addressing the problem of their transient existence. Analogous to 3D objects with spatial dimensions on three orthogonal axes, we have added three angular momenta along three orthogonal axes of an electromagnetic energy packet to create a 3D shape of fields. Design optimization of synthetic organic helical nanowires was used to control the passage of incident photons so that three mutually perpendicular dipolar forces create a hollow sphere of light by interference [11–15]. These condensate-like photonic structures interfere like waves and disintegrate into constituent photonic structures; light structure does break into pieces. Dimensionless photons acquire dimensions and form and create non-dissipative ripples in spacetime curvature that might be tuned using an applied electromagnetic signal, such as radio or microwaves. Vortices are known to interfere, which could be used to build complex structures, including knots of darkness [16–18] and complex phase structures for quantum computing [19–21], however, the engineering of optical vortices has been primarily limited to two dimensions [22–25]. Here, an explicit theory is built and experimentally verified [26] to universally design a 3D matrix of three interconnected helical nanowires that naturally generates a standalone 3D vortex. The same design protocol can be used to create system invariant virtual particles of different fields, from turbulences in the atomic knots [27] to the quantum fluids [28].

Here, we have transformed a dimensionless photon into a cavity-free standalone vortex structure under ambient conditions using a light–matter interaction that condenses photons to acquire a volume, which can be superposed to obtain both wave-like interference and particle-like disintegration. A 3D template is used where electron density distributes in an intricate 3D path [22] wherein incident photons experience three orthogonal fields as they interact with matter. Templates for light–matter interaction have so far been constructed using only 2D surfaces, with curves having dimensions of the order of wavelength to reshape waveform using only the reflection of light [23,24]. For the 3D semitransparent cavity used here, photons do not reflect but refract and transmit through the overlapping cavity boundaries. In contrast to the surfaces of the existing 2D templates, the entire cavity is engaged in reshaping the emitted photon. If designed suitably, the emitted photon's structure resembles the shape of the template it passes through. The unprecedented three-mode interactions of photons with three dimensions of matter make possible the design of a cavity that resembles the expected singularity region of the reshaped photon post-light–matter interaction.

A phase singularity is neither zero nor an astronomically large value; it is an undefined entity when the phase gradient varies arbitrarily in space. Adding an angular momentum requires encoding a phase singularity in the wavefront in a particular direction [11–13]. However, the simultaneous encoding of three-phase singularities in the three perpendicular directions is not known. Light interacts with the electron density distribution of a material [14] so that the object's surface morphology modulates the vortices of the emitted photons and affects the singularity regions [15].

Figure 1A shows a helical nanowire wherein energy would take a spiral path, leaving a central core similar to an empty space encoded as a phase singularity region when an incident photon adopts a spiral route during transmission through the helical electron density distribution path. Projected light is then not a dot with orbital angular momentum θ; it is a ring of light known as an optical vortex. Figure 1B shows a spiral of a spiral where the singularity region is a helical tube. Incident photons split into two entangled photon sources and interfere, creating alternate dark and bright spots on the projected ring of light, and we obtain a radial angular momentum ϕ. Figure 1C illustrates the seminal work of Nye, who demonstrated mathematically that a twisted helix or a helix of a helix could emit particle-like standalone optical vortices [25] (see Visualization 1). For this reason, we opted to use a twisted helix, similar to that naturally abundant in microtubules or DNA. Here, incident photons experience three orthogonal electron density distributions; three perpendicular forces rotate the optical vortex centrifugally to obtain the third centrifugal angular momentum ω as a hollow sphere of light. The dark regions on the particle-like sphere of light are singularity regions; system points move along the borderline between dark and bright regions as constituents of final optical condensate, represented by a single wave function $\Psi(\theta, \phi, \omega)$. Face-to-face collision between a pair of vortices generated in water forms small vortices at the ring perimeter [26]. We have repeated that experiment here using light vortices to disintegrate the wave function of the entire condensate and create a ring of light with dark and bright spots. The light condensate is a single particle that exhibits both interference like a wave and disintegration like a particle.

Since the shape of a cavity or template and cavity-modified photon is similar, we have used a three-level self-assembly in which molecules first form a spiral structure with a diameter of ~15–20 nm (Methods, *online*). The resulting spiral structure then self-assembles into a larger helix with a diameter of ~120 nm, which finally forms as a hierarchically structured helix with a diameter of ~12 µm. We have also studied this reaction environment using computer simulations [28,29]. With increasing numbers of molecules in the self-assembly simulations, three orthogonal phase transitions occur as constituent molecular structures bind (Figure 2A, see Visualization 2). Incorporating such 3D dynamics requires a tensor to express all states Ψ on a spherical optical surface, $\Psi(\theta, \phi, \omega) = Cos\theta Sin\omega + e^{i\phi} Sin\theta Cos\omega$. A plot of this function has the form of a triplet of teardrops oriented on 120° solid angular planes (Figure 2B, right). The optical surface

is the phase surface. We insert a pair of electrodes into the reaction vessel to measure signals during the three phase transitions. The connected spectrum analyzer shows a triplet of resonance frequencies. To estimate the dimensions of the self-assembled structures as they evolve through the three transmission modes, we focused a camera on the reaction vessel to detect diffracted nano-micro-particles at nucleation centers as the precursor solution cooled. Simultaneously, a polarized He-Ne laser (beam cross-section: 1 mm^2) was transmitted through the nucleation centers and projected on a screen, where a projection camera captured the sequence of events. First, birefringence—or a pair of light spots—is observed above ~10 nm particle size [30] (Figure S2), then fast flashing of light spheres occurs for 0.01 s, followed by the appearance of an interference pattern of parallel beams. This is the first optical vortex based on an orbital angular momentum. Subsequently, the initially formed vortex disappears, with no transmission visible at the projection screen, and no diffused particles are detected in the reaction vessel camera. We refer to this dark state as a metastable state. Following this state, particles reappear and converge, and we observe photons with a radial angular momentum. A second subsequent metastable state is followed finally by forming the third condensate, consisting of a sphere of light. From scanning electron micrographs (SEM), we match the size of objects generating light diffraction to assess the most probable appearance of nanowire assemblies that generate photon structures with one, two, or three angular momenta (see Visualization 3 and its description (Text S4 online. Visualization 3)).

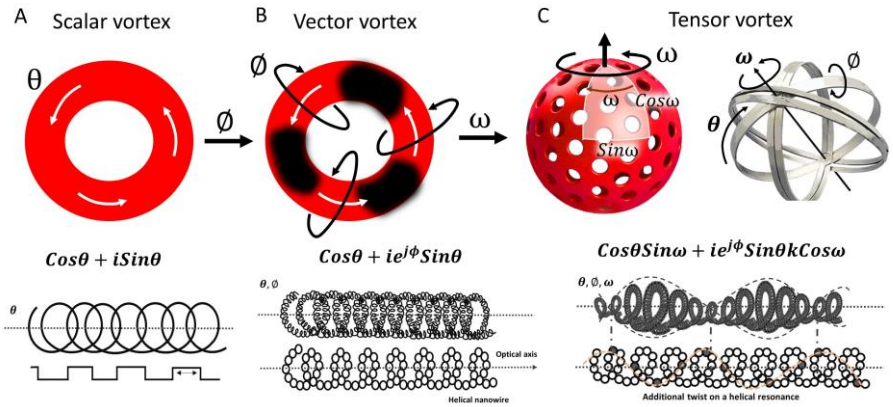

Figure 1. A generic engineering principle to synthesize optical structures having three angular momenta. The transition from (**A**) a scalar vortex (θ) to (**B**) a vector vortex (θ, ϕ) then to (**C**) a tensor vortex or a 3D optical sphere $\Psi(\theta, \phi, \omega)$ is depicted. In each panel, the top row shows vortices projected on a screen, the middle row indicates the photon transmission pathway, and the bottom row shows the electron density distribution path in a template that regulates light-matter interaction to generate a particular vortex shape. Three complex functions describe the 1D, 2D, and 3D optical vortices. In panel (**C**) (lower part), a black dot on the helix indicates the added periodicity in the electron density distribution to create the helix of a helix described by Nye [25].

Since the cavity shape for light–matter interaction and a reshaped photon with three angular momenta are similar, both emitted photon condensate and organic condensate responsible for its formation have the same energy expression or Hamiltonian H. Four light–matter interactions dominate refraction and transmission in a twisted helix to render volume to a photon by adding a third angular momentum. Synthesis of self-similar helical-symmetry-based superstructures have been grown spontaneously using self-assembly from the nano-scale to the visible scale [31]. The organic twisted helix structure that generates photon condensate was recreated in a Computer Science and Technology (CST) simulator. Four key features were noted and included in H = H1 + H2 + H3 + H4 (Figure S1a,b, Text S1A). An electromagnetic field flowing in a loop on the helix with multiple parallel pathways of electron density loops maintaining an energy gap. Quantized flux exchanges between the loops, where each loop acts as a distinct energy level (H1). H1

regulates the refraction of photons. The orientations of helical nanowires in three layers grown from a triplet of precursor molecules are directed in different directions, leading to the anisotropy of energy flow in transmission (H2). Refracted and transmitted parts governed by geometric parameters of the twisted helix, length, pitch, diameter, and lattice area act as two distinct coherent sources, which interfere and generate a 3D vortex (H3). The additional twist in the coil, which Nye has proposed would generate free 2D light structures, is implemented here by using an organic structure containing screw and edge dislocations [25] and eventually governs the shape of singularity regions (H4, Figure S1c). The function $\Gamma_i(r,t) = 3\sum_i cosx_i + 4\prod_i cosx_i$ includes three periodic variations of electron density of states along three orthogonal axes, which could have at most 12 singularity regions on the hollow sphere (Figure S1b). Complex singularity regions have already been realized using femtosecond pulses [32]. For θ, a photon's azimuthal angular momentum is $l\hbar$; for ϕ, its radial angular momentum is $p\hbar$; for ω, centrifugal angular momentum is $o\hbar$; here, (l, p, o) are topological charges. Since all twelve values on a sphere follow $-\pi \leq \Gamma_i(r,t) \leq +\pi$, the third angular momentum of the largest dark region is ~$0.2\pi\hbar$ kg m^2/sec. This suggests a complex knot structure [33].

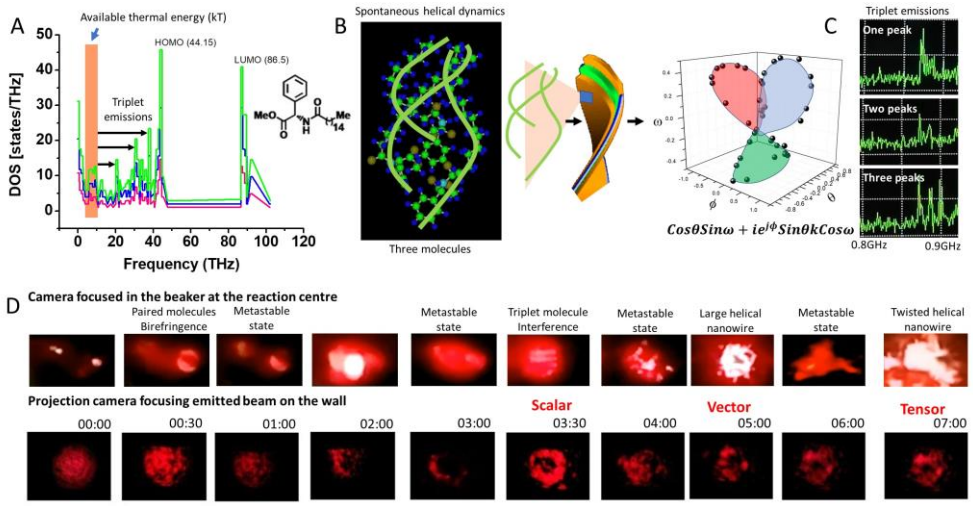

Figure 2. Triplet resonance bands drive molecular self-assembly suitable for three angular momenta of a photon. (**A**) Density of states of the single, double, and triple molecular precursors (IUPAC Name (S) −Phenyl-hexadecanoylamino-acetic acid methyl ester) are plotted as a function of energy (THz) as molecular dynamics simulation runs in a potential box (see Visualization 2). Resonance frequencies are the highest−energy density peaks derived at HOMO and LUMO levels. The band for interacting with available free thermal noise (5−6 THz) is highlighted in orange. Three arrows indicate HOMO + 1, HOMO + 2, and HOMO + 3 from the kT band. (**B**) Screenshot depicts a naturally forming helical triplet from Visualization 2 (left). From this structure, higher−order triplet self-assembly is observed on the micrometer to millimeter scale (immediate right). At most right, function $Cos\theta Cos\omega + ie^{j\phi} Sin\theta Sin\omega$ is plotted for three variables θ, ϕ, ω. Three loops are at 120° solid angles and symmetrically oriented in a virtual 3D sphere. (**C**) Spectrum analyzer measures transmission coefficients ($S_{21}-S_{12}$) in situ across the helical nanowire superstructure. (**D**) Two time profiles of pure light diffracted (top) and reflected, transmitted, and refracted by growing structure as precursor molecules form 1D nanowire to helically twisted structures. Live visualization of four distinct phase transitions and metastable states as observed using the reaction vessel camera (top, Visualization 3) and optical vortex condensate formation observed using the projection camera (bottom, Visualization 4). The actual size of optical structures is 5 μm × 5 μm in the beaker, and when they are magnified using a lens and projected on a wall and presented here, they are 10 cm × 10 cm (each window size of Figure 2D).

We rotated the reaction vessel in which helical nanowires form and reorganize, counted the dark or singularity regions on the light sphere, and estimated their shapes (Figure 3A).

On the projected hollow light sphere, there exist either polygons, whose vertices are composed of a framework of light columns or circular dark regions whose perimeters are composed of light rings. Two parts, the front and back of the light structure, are detected separately; taken together, we confirm that it is a standalone structure (Figure 3B top). Three time profiles of magnetic flux variations on the projected vortex along three orthogonal directions of its posterior reveal streams of spherical pulses (Figure 3B bottom). Thus, the gel produces a linear chain of free optical structures under ambient conditions. We repeatedly dissolved the gel superstructure by heating it at 75 °C, cooled it to reform, and observed the number of dark regions, n, their areas, and the average distances $\langle x \rangle$ between regional centers (see Visualization 4, Figure 3C, Text S1 B). This process was repeated exhaustively for different gels, revealing that the geometric arrangements of dark regions on the light sphere are not random but are specific to gel precursor molecules (Table S1). The n vs. pitch/diameter plot for helical nanowires shows that the dark regions of 3D light structures are linked to the structural symmetry of the helical nanowire assembly (Figure 3D). We also used mirrors to reflect the optical superstructure with the gel-containing reaction vessel fixed; each dark region is the constituent photon's phase sphere (Figure 3D). Incident photons interact with the characteristic length, pitch, and diameter of the hierarchical nanowire network, and the resulting dark regions map Bloch spheres connected by geometric shapes. Table S1 (Text S2) shows the 3D assembly of Bloch spheres or topology of multiple vortices representing each gel [34].

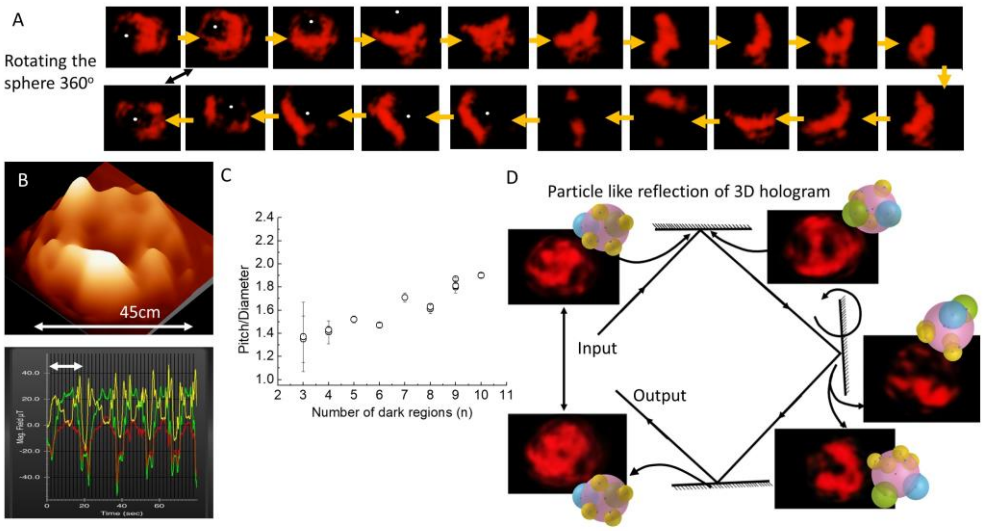

Figure 3. Confirmation of particle-like 3D morphology of the optical vortex condensate. (**A**) Variation in the vortex shape observed using the projection camera, as helical nanowire assembly is rotated by rotating the vessel. White dot placed at a selected light loop on the sphere confirms its return to origin following a 360° rotation (see Visualization 4). (**B**) Optical vortex condensate is projected on a screen 7 m distant (top), in order to measure positional values (x,y,z) and its corresponding magnetic flux values (red, green, yellow) in microtesla (bottom). The scanner is moved periodically back and forth across the structure, and the magnetic flux values capture five periods. Extent of a single period is indicated by the arrow. (**C**) Ratio of pitch and diameter for six gels with the number of dark domains on the sphere. (**D**) Vortex images captured by rotating sample and mirror reflection separately to eliminate the possibility that the 3D vortex is the half-sphere of a Gaussian wave packet. 360° rotation of the sphere regenerates the same pattern in input and output. 3D assembly of Bloch spheres shown adjacent to a rotational phase hologram is an invariant 3D sphere networks formed by theoretically simulating the holographic laser projection from H. Geometrically connected Bloch spheres measures phase on the surface of a host Bloch sphere. The actual size of optical structures is 5 μm × 5 μm in the beaker, and when they are magnified using a lens and projected on a wall and presented here, they are 10 cm × 10 cm (each window size of all panels).

To provide further evidence that the sphere of light is a unit photon structure with three angular momenta, we passed two entangled photons at 90° out-of-phase through two gel solutions (see Figure 4A,B). The two gels emit two optical superstructures as vortex spheres. We interfered the optical spheres at a beam splitter junction by two methods: first at 45°, then by orienting the splitter further by 90°. A Canada balsam layer joins the two parts of the beam splitter. Here, the layer thickness was adjusted to the He-Ne laser wavelength to split the photon into two parts, one reflected and the other transmitted due to evanescent wave coupling as frustrated total internal reflection (FTIR). We could select whether vortex spheres superpose at the junction on the same or opposite side during interference. In the first protocol, two spherical vortices pass through one common part of the beam splitter and interfere at the junction surface. Since two vortex spheres do not cross the junction, this is a reflection mode superposition (Figure 4A). Second, two vortices enter from two sides of the beam splitter and arrive at the same point inside the Canada balsam junction. Since the vortex spheres must cross the junction for interference, we achieve transmission mode superposition (Figure 4B). Due to FTIR, these two interferences use different energy regions of the same vortex sphere.

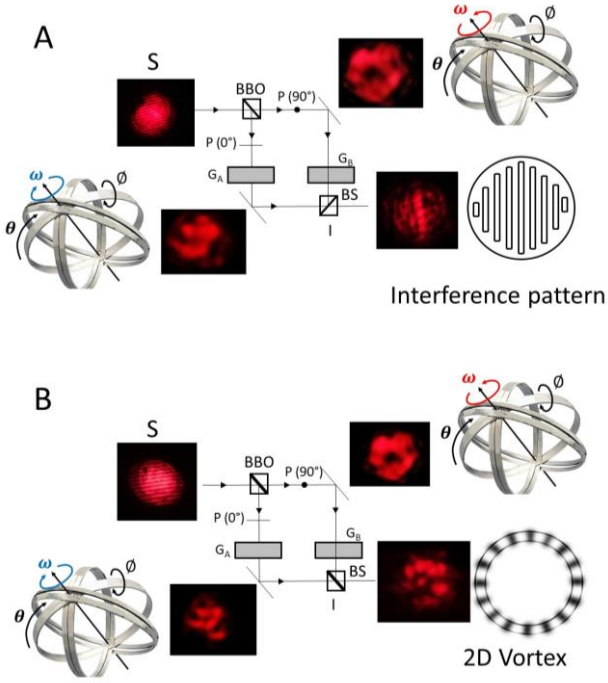

Figure 4. Wave-particle duality of the photon condensate or optical 3D sphere. In panels (**A**,**B**), an interferometer where He-Ne laser source S is split into two entangled components by a beam splitter (two β-Barium Borate or BBO crystals fixed together) was used. Two 90° out-of-phase polarizers filter out two different parts, which pass through different gel solutions G_A and G_B, generating two vortices with $+\omega$ and $-\omega$ parts (green clockwise, red counter-clockwise), interfered at the beam splitter BS acting as interferometer I. For Panel (**A**), the output is taken as an interference pattern, and for panel (**B**), the output is taken as a 2D vortex. The only difference between the experimental setup for panel (**A**) and panel (**B**) is the orientation of the junction of the two parts of the beam splitter assigned as interferometer I. The actual size of optical structures is 5 μm × 5 μm in the beaker, and when they are magnified using a lens and projected on a wall and presented here, they are 10 cm × 10 cm (each window size all panels).

In reflection mode, both spheres arrive at the same side of the splitter and interfere. A wave-like interference is observed with parallel grids of constructive and destructive interference visible (Figure 4A). However, when both beams of $\Psi(\theta, \phi, \omega)$—namely, A $(\theta,\ \phi,\ \omega)$ and B $(\theta, \phi, -\omega)$—arrive at the same point following the transmission mode through the different sides of a beam splitter, then one of the angular momenta is eliminated

and the output returns as the optical vortex beam (A + B = $\Psi(\theta, \phi)$; Figure 4B). Therefore, we can derive a photon with two angular momenta from a photon having three angular momenta. Disintegrating 3D photons into 2D photon-fragments is quite similar to the collision of water ripples [26]. It is a new type of wave–particle duality. To create A and B, the entangled photons are made 90° out-of-phase using paired BBO crystals before being made incident on the gel solution. Polarization of photons does not affect scalar and vector angular momenta. However, it changes the direction of the twist of twists, i.e., the tensor angular momentum ω, resulting in two spherical vortices or photon condensates, ω and $-\omega$. Since the twist of a twist effect resulting in $\pm\omega$ is canceled, one of the three emitted vortices is observed as a vector vortex beam ϕ. It is possible to fine-tune the collapsed 2D vortices obtained by colliding the optical spheres. We can then select and edit one of the twelve topological quantum states, each with a distinct clocking direction embedded in the optical sphere, using $\Gamma_i(r, t)$.

Using the third angular momentum, one can reshape the photon's waveform into a standalone structure. By tuning the light sphere or ellipsoid's diameter or distance between two endpoints at which the intensity of the waveform becomes zero, it is possible to precisely regulate the pressure exerted by a 3D photon stream. Furthermore, by adjusting the singularity area, particles might be encapsulated in the hollow sphere for transportation. Mass transport using light could be possible in the future using 3D optical structures. The free particle-like complex photon structure derived by Nye is used here to create a template for light–matter interaction [25]. However, using that unique light–matter interaction, the existing idea of using a 2D template that reflects a photon is replaced here by a 3D template that refracts and transmits a look-alike photon. Introduction to 3D-template-based engineering of light would open the door to more complex structures of light that could memorize codes to instruct and operate machines at a remote distance and build circuit-less, algorithm-free computers [35]. One of the most important outcomes of the 3D template engineering is the use of birefringence, which generates entangled photons in a hydrogen-bonded nanowire-made cavity that vibrates to condense photons into an integrated form. Entangled photons are fused to create a single photon structure; this is the basic engineering for organic-gel-based quantum computers, quantum cryptography, reverse engineering of polyatomic time crystals [36], brain inspired computing [37], etc. Therein, geometric shapes made of coupled quantum states or Bloch spheres are editable in a particle-like photonic structure whose shape would be fairly similar to the cavity that the photon encounters. Therefore, one would design templates, and the resultant photon structure would look like the template.

Supplementary Materials: The following supporting information can be downloaded at: https://www.mdpi.com/article/10.3390/sym15010158/s1. S1. Materials and Methods; A. Preparation of Gelators; B. Birefringence and optical vortex study. S2. Supplementary Texts; 2.1. Hamiltonian of the helical nanowire; 2.2. Optical interaction with the helical nanowire: 2.3. Measuring third angular momentum for seventeen gels: S3. Supplementary Figures; Figure S1. Hamiltonian for gel's light–matter interaction; Figure S2. Birefringence of a helical nanowire. Table S1; Nested Bloch spheres or Hilbert spaces for six organic gel precursors. S4. Four visualization descriptions; Visualization 1: Basic concept for third angular momentum, Visualization 2: Molecular dynamics of gel precursors. Visualization 3: Four phase transitions for vortex condensate, Visualization 4: Statistical database of repeated experiments. S5. References [38–58].

Author Contributions: Conceptualization, A.B.; data curation, P.S. (Pathik Sahoo); formal analysis, P.S. (Pathik Sahoo) and P.S. (Pushpendra Singh); funding acquisition, A.B.; investigation, A.B.; methodology, P.S. (Pathik Sahoo) and J.M.; software, P.S. (Pushpendra Singh); supervision, A.B.; writing—original draft, A.B.; writing—review and editing, P.S. (Pathik Sahoo), P.S. (Pushpendra Singh), J.M., R.P.S., J.P.H., T.N., S.G. and A.B. All authors have read and agreed to the published version of the manuscript.

Funding: The authors acknowledge the Asian Office of Aerospace R&D (AOARD), a part of the United States Air Force (USAF), for Grant no. FA2386-16-1-0003 (2016–2019) on electromagnetic resonance-based communication and intelligence of biomaterials.

Data Availability Statement: See Supplemental Document for supporting content.

Acknowledgments: The authors acknowledge the Asian Office of Aerospace R&D (AOARD), a part of the United States Air Force (USAF), for Grant no. FA2386-16-1-0003 (2016–2019) on electromagnetic resonance-based communication and intelligence of biomaterials. This work was partly supported by World Premier International Research Center Initiative (WPI Initiative), MEXT, Japan.

Conflicts of Interest: The authors declare that they have no competing financial or non-financial interests.

References

1. Everitt, C.W.F.; DeBra, D.B.; Parkinson, B.W.; Turneaure, J.P.; Conklin, J.W.; Heifetz, M.I.; Keiser, G.M.; Silbergleit, A.S.; Holmes, T.; Kolodziejczak, J.; et al. Gravity Probe B: Final Results of a Space Experiment to Test General Relativity. *Phys. Rev. Lett.* **2011**, *106*, 221101. [CrossRef] [PubMed]
2. Harada, K.; Matsuda, T.; Bonevich, J.; Igarashi, M.; Kondo, S.; Pozzi, G.; Kawabe, U.; Tonomura, A. Real-time observation of vortex lattices in a superconductor by electron microscopy. *Nature* **1992**, *360*, 51–53. [CrossRef]
3. Christoph, J.; Chebbok, M.; Richter, C.; Schröder-Schetelig, J.; Bittihn, P.; Stein, S.; Uzelac, I.; Fenton, F.H.; Hasenfuß, G.; Gilmour, R.F.; et al. Electromechanical vortex filaments during cardiac fibrillation. *Nature* **2018**, *555*, 667–672. [CrossRef] [PubMed]
4. Dorrah, A.H.; Rubin, N.A.; Tamagnone, M.; Zaidi, A.; Capasso, F. Structuring total angular momentum of light along the propagation direction with polarization-controlled meta-optics. *Nat. Commun.* **2021**, *12*, 6249. [CrossRef]
5. Aiello, A.; Banzer, P.; Neugebauer, M.; Leuchs, G. From transverse angular momentum to photonic wheels. *Nat. Photonics* **2015**, *9*, 789–795. [CrossRef]
6. Berry, M.V.; Dennis, M.R. Topological events on wave dislocation lines: Birth and death of loops, and reconnection. *J. Phys. A Math. Theor.* **2006**, *40*, 65–74. [CrossRef]
7. Forbes, A. Modern tools for classical and quantum communication with vector vortex beams. In Proceedings of the 2018 23rd Opto-Electronics and Communications Conference (OECC), Jeju, Republic of Korea, 2–6 July 2018; pp. 1–2. [CrossRef]
8. Rego, L.; Dorney, K.M.; Brooks, N.J.; Nguyen, Q.L.; Liao, C.-T.; Román, J.S.; Couch, D.E.; Liu, A.; Pisanty, E.; Lewenstein, M.; et al. Generation of extreme-ultraviolet beams with time-varying orbital angular momentum. *Science* **2019**, *364*, eaaw9486. [CrossRef]
9. D'Ambrosio, V.; Carvacho, G.; Graffitti, F.; Vitelli, C.; Piccirillo, B.; Marrucci, L.; Sciarrino, F. Entangled vector vortex beams. *Phys. Rev. A* **2016**, *94*, 030304. [CrossRef]
10. Taylor, A.J.; Dennis, M.R. Vortex knots in tangled quantum eigenfunctions. *Nat. Commun.* **2016**, *7*, 12346. [CrossRef]
11. Lim, S.W.D.; Park, J.-S.; Meretska, M.L.; Dorrah, A.H.; Capasso, F. Engineering phase and polarization singularity sheets. *Nat. Commun.* **2021**, *12*, 4190. [CrossRef]
12. Taira, Y.; Zhang, S. Split in phase singularities of an optical vortex by off-axis diffraction through a simple circular aperture. *Opt. Lett.* **2017**, *42*, 1373–1376. [CrossRef] [PubMed]
13. Ruchi; Senthilkumaran, P.; Pal, S.K. Phase Singularities to Polarization Singularities. *Int. J. Opt.* **2020**, *2020*, 1–33. [CrossRef]
14. Albini, F.A.; Jahn, R.G. Reflection and Transmission of Electromagnetic Waves at Electron Density Gradients. *J. Appl. Phys.* **1961**, *32*, 75–82. [CrossRef]
15. Dutreix, C.; Bellec, M.; Delplace, P.; Mortessagne, F. Wavefront dislocations reveal the topology of quasi-1D photonic insulators. *Nat. Commun.* **2021**, *12*, 3571. [CrossRef] [PubMed]
16. Leach, J.; Dennis, M.R.; Courtial, J.; Padgett, M.J. Knotted threads of darkness. *Nature* **2004**, *432*, 165. [CrossRef]
17. Berry, M. Making waves in physics: Three wave singularities from the miraculous 1830s. *Nature* **2000**, *403*, 21. [CrossRef]
18. O'Holleran, K.; Padgett, M.; Dennis, M.R. Topology of optical vortex lines formed by the interference of three, four, and five plane waves. *Opt. Express* **2006**, *14*, 3039–3044. [CrossRef] [PubMed]
19. Frolov, S. Quantum computing's reproducibility crisis: Majorana fermions. *Nature* **2021**, *592*, 350–352. [CrossRef]
20. Mosseri, R.; Dandoloff, R. Geometry of entangled states, Bloch spheres and Hopf fibrations. *J. Phys. A Math. Gen.* **2001**, *34*, 10243–10252. [CrossRef]
21. Wie, C.-R. Two-Qubit Bloch Sphere. *Physics* **2020**, *2*, 383–396. [CrossRef]
22. Huang, C.; Chen, X.; Oladipo, A.O.; Panoiu, N.C.; Ye, F. Generation of Subwavelength Plasmonic Nanovortices via Helically Corrugated Metallic Nanowires. *Sci. Rep.* **2015**, *5*, 13089. [CrossRef]
23. Yu, N.; Capasso, F. Flat optics with designer metasurfaces. *Nat. Mater.* **2014**, *13*, 139–150. [CrossRef] [PubMed]
24. Ye, J.; Li, Y.; Liu, Y.; Qu, S. On-Chip Optical Vortex Generation and Topological Charge Control by Methods of Wave Vector Manipulation. *IEEE Photonics J.* **2022**, *14*, 1–7. [CrossRef]
25. Nye, J.F. Polarization effects in the diffraction of electromagnetic waves: The role of disclinations. *Proc. R. Soc. London Ser. A Math. Phys. Sci.* **1983**, *387*, 105–132. [CrossRef]
26. Lim, T.T.; Nickels, T.B. Instability and reconnection in the head-on collision of two vortex rings. *Nature* **1992**, *357*, 225–227. [CrossRef]

27. Kragh, H. The Vortex Atom: A Victorian Theory of Everything. *Centaurus* **2002**, *44*, 32–114. [CrossRef]
28. Tang, Y.; Bao, S.; Guo, W. Superdiffusion of quantized vortices uncovering scaling laws in quantum turbulence. *Proc. Natl. Acad. Sci. USA* **2021**, *118*, e2021957118. [CrossRef]
29. Froeyen, M.; Abu el Asrar, R.; Abramov, M.; Herdewijn, P. Molecular simulation of cyclohexanyl nucleic acid (CNA) duplexes with CNA, DNA and RNA and CNA triloop and tetraloop hairpin structures. *Bioorganic Med. Chem.* **2016**, *24*, 1778–1785. [CrossRef]
30. Oldenbourg, R.; Salmon, E.; Tran, P. Birefringence of Single and Bundled Microtubules. *Biophys. J.* **1998**, *74*, 645–654. [CrossRef]
31. Ghosh, S.; Dutta, M.; Ray, K.; Fujita, D.; Bandyopadhyay, A. A simultaneous one pot synthesis of two fractal structures via swapping two fractal reaction kinetic states. *Phys. Chem. Chem. Phys.* **2016**, *18*, 14772–14775. [CrossRef]
32. Xu, L.; Li, D.; Chang, J.; Li, D.; Xi, T.; Hao, Z. Powerful supercontinuum vortices generated by femtosecond vortex beams with thin plates. *Photonics Res.* **2022**, *10*, 802–809. [CrossRef]
33. Zhong, J.; Liu, S.; Guo, X.; Li, P.; Wei, B.; Han, L.; Qi, S.; Zhao, J. Observation of optical vortex knots and links associated with topological charge. *Opt. Express* **2021**, *29*, 38849. [CrossRef] [PubMed]
34. Das, P.; Tasgin, M.E.; Müstecaplıoğlu, E. Collectively induced many-vortices topology via rotatory Dicke quantum phase transition. *New J. Phys.* **2016**, *18*, 093022. [CrossRef]
35. Ghosh, S.; Fujita, D.; Bandyopadhyay, A. An organic jelly made fractal logic gate with an infinite truth table. *Sci. Rep.* **2015**, *5*, 1–8. [CrossRef] [PubMed]
36. Saxena, K.; Singh, P.; Sarkar, J.; Sahoo, P.; Ghosh, S.; Krishnananda, S.D.; Bandyopadhyay, A. Polyatomic time crystals of the brain neuron extracted microtubule are projected like a hologram meters away. *J. Appl. Phys.* **2022**, *132*, 194401. [CrossRef]
37. Singh, P.; Saxena, K.; Singhania, A.; Sahoo, P.; Ghosh, S.; Chhajed, R.; Ray, K.; Fujita, D.; Bandyopadhyay, A. A Self-Operating Time Crystal Model of the Human Brain: Can We Replace Entire Brain Hardware with a 3D Fractal Architecture of Clocks Alone? *Information* **2020**, *11*, 238. [CrossRef]
38. Karnieli, A.; Arie, A. Fully controllable adiabatic geometric phase in nonlinear optics. *Opt. Express* **2018**, *26*, 4920–4932. [CrossRef]
39. Slussarenko, S.; Alberucci, A.; Jisha, C.; Piccirillo, B.; Santamato, E.; Assanto, G.; Marrucci, L. Guiding light via geometric phases. *Nat. Photonics* **2016**, *10*, 571–575. [CrossRef]
40. Kuznetsov, A.I.; Miroshnichenko, A.E.; Brongersma, M.L.; Kivshar, Y.S.; Luk'yanchuk, B. Optically resonant dielectric nanostructures. *Science* **2016**, *354*, aag2472. [CrossRef]
41. Wang, J.; Yang, J.-Y.; Fazal, I.M.; Ahmed, N.; Yan, Y.; Huang, H.; Ren, Y.; Yue, Y.; Dolinar, S.; Tur, M.; et al. Terabit free-space data transmission employing orbital angular momentum multiplexing. *Nat. Photonics* **2012**, *6*, 488–496. [CrossRef]
42. Bozinovic, N.; Yue, Y.; Ren, Y.; Tur, M.; Kristensen, P.; Huang, H.; Willner, A.E.; Ramachandran, S. Terabit-Scale Orbital Angular Momentum Mode Division Multiplexing in Fibers. *Science* **2013**, *340*, 1545–1548. [CrossRef] [PubMed]
43. Maurer, C.; Jesacher, A.; Bernet, S.; Ritsch-Marte, M. What spatial light modulators can do for optical microscopy. *Laser Photonics Rev.* **2011**, *5*, 81–101. [CrossRef]
44. Chakraborty, S.; Bhattacharya, K.; Sarkar, S.K. Quantitative birefringence microscopy with collinearly propagating orthogonally polarized beams. *Appl. Opt.* **2018**, *57*, 1934–1939. [CrossRef]
45. Mair, A.; Vaziri, A.; Weihs, G.; Zeilinger, A. Entanglement of the orbital angular momentum states of photons. *Nature* **2001**, *412*, 313–316. [CrossRef] [PubMed]
46. Leach, J.; Jack, B.; Romero, J.; Jha, A.K.; Yao, A.M.; Franke-Arnold, S.; Ireland, D.G.; Boyd, R.W.; Barnett, S.M.; Padgett, M.J. Quantum Correlations in Optical Angle-Orbital Angular Momentum Variables. *Science* **2010**, *329*, 662–665. [CrossRef]
47. Terech, P.; Ostuni, E.; Weiss, R.G. Structural Study of Cholesteryl Anthraquinone-2-carboxylate (CAQ) Physical Organogels by Neutron and X-ray Small Angle Scattering. *J. Phys. Chem.* **1996**, *100*, 3759–3766. [CrossRef]
48. Basak, S.; Nanda, J.; Banerjee, A. A New Aromatic Amino Acid Based Organogel for Oil Spill Recovery. *J. Mater. Chem.* **2012**, *22*, 11658–11664. [CrossRef]
49. Nagao, Y.; Yagi, M.; Ikede, T.; Fujita, E. A New Chiral Recognition in Aminolysis of 3-Acyl-4(R)-methoxycarbonyl-1,3-thiazolidine-2-thione with Racemic Amines. *Tetrahedron Lett.* **1982**, *23*, 201–204. [CrossRef]
50. Ongaratto, R.; Conte, N.; D'Oca, C.R.M.; Brinkerhoff, R.C.; Ruas, C.P.; Gelesky, M.A.; D'Oca, M.G.M. In Situ Formation of AuNPs using Fatty N-Acylamino Hydrazide Organogelators as Templates. *New J. Chem.* **2019**, *43*, 295–303. [CrossRef]
51. Pal, A.; Ghosh, Y.K.; Bhattacharya, S. Molecular Mechanism of Physical Gelation of Hydrocarbons by Fatty Acid Amides of Natural Amino Acids. *Tetrahedron* **2007**, *63*, 7334–7348. [CrossRef]
52. Thalhammer, A.; Mecinović, J.; Schofield, C.J. Triflic Anhydride-mediated Synthesis of Oxazoles. *Tetrahedron Lett.* **2009**, *50*, 1045–1047. [CrossRef]
53. Ordóñez, M.; Hernández-Fernández, E.; Montiel-Pérez, M.; Bautista, R.; Bustos, P.; Rojas-Cabrera, H.; Fernández-Zertuche, M.; García-Barradas, O. A Convenient Method for the Preparation of Chiral Phosphonoacetamides and their Horner-Wadsworth-Emmons Reaction. *Tetrahedron Asymmetry* **2007**, *18*, 2427–2436. [CrossRef]
54. Bender, M. The use of light scattering to determine particle size and molecular weight and shape. *J. Chem. Educ.* **1952**, *29*, 15–23. [CrossRef]
55. Ye, Y.; Pui, D.Y.H. Detection of nanoparticles suspended in a light scattering medium. *Sci. Rep.* **2011**, *11*, 20268. [CrossRef] [PubMed]
56. Kumar, A.; Taneja, A.; Mohanty, T.; Singh, R.P. Effect of laser beam propagation through the plasmonic nanoparticles suspension. *Results Opt.* **2021**, *3*, 100081. [CrossRef]

57. Yang, Z.Y.; Zhao, M.; Lu, P.X.; Lu, Y.F. Ultrabroadband optical circular polarizers consisting of double-helical nanowire structures. *Opt. Lett.* **2010**, *35*, 2588–2590. [CrossRef] [PubMed]
58. Esposito, M.; Tasco, V.; Cuscunà, M.; Todisco, F.; Benedetti, A.; Tarantini, I.; De Giorgi, M.; Sanvitto, D.; Passaseo, A. Nanoscale 3D chiral plasmonic helices with circular dichroism at visible frequencies. *ACS Photonics* **2015**, *2*, 105–114. [CrossRef]